Scientific Research Publishing

Journal of Quantum Information Science, 2022, 12, 111-124
https://www.scirp.org/journal/jqis
ISSN Online: 2162-576X
ISSN Print: 2162-5751

The Superconductivity in Fe-Based Family of Superconductors and Its Electronic Structure Analysis in Presence of Dopants Rh and Pd

Ronald Columbié-Leyva[1], Alberto López-Vivas[1†], Ulises Miranda[2], Ilya G. Kaplan[1*]

[1]Instituto de Investigación en Materiales, UNAM, CDMX, México
[2]Baltic Scientific Instruments, Riga, Latvia
Email: *kaplan@unam.mx

How to cite this paper: Columbié-Leyva, R., López-Vivas, A., Miranda, U. and Kaplan, I.G. (2022) The Superconductivity in Fe-Based Family of Superconductors and Its Electronic Structure Analysis in Presence of Dopants Rh and Pd. *Journal of Quantum Information Science*, **12**, 111-124.
https://doi.org/10.4236/jqis.2022.124010

Received: November 11, 2022
Accepted: December 26, 2022
Published: December 29, 2022

Abstract

The discovered in 2008 Fe-based superconductors (SC) are a paramagnetic semimetal at ambient temperature and in some cases they become superconductor upon doping. In spite of so many years since its discovery it is still not known the mechanism that leads to superconductivity. The electronic structure study is used for determining key features of the SC mechanism in these materials. The calculations were performed using the modern suite of programs MOLPRO 2021. We performed quantum calculations of a cluster embedded in a background charge distribution that represents the infinite crystal. The Natural Population Analysis was used for determining the charge and spin distribution in the studied materials. As follows from our results, the possible mechanism for superconductivity corresponds to the RVB theory proposed by Anderson for high T_c superconductivity in cuprates.

Keywords

Iron-Based High-T_c Superconductors, Superconductivity, Embeded Cluster Method, Natural Bonding Orbitals Analysis

1. Introduction

The superconductivity (SC) in the Hg at very low temperatures, T_c = 4.19 K, was discovered in 1911 Kamerlingh Onnes [1]. For explaining the SC phenomenon, it was required the quantum mechanical conceptions. The quantum mechanics was created by Heisenberg, Born and Jordan [2] [3] in 1925-1926. After, Schrödinger [4] [5] introduced the wave function ψ for describing the

†Alberto Lopez-Vivas recently died during our work on the current paper, we would like to express our gratitude for his contributions.

microparticles and formulated his famous wave equation.

The Iron based superconductors (IBSC) were discovered in the next century, in 2008, by Hosono and coworkers [6] [7]. They are characterized into six different families [8]. Among them, the 122 Ba-based family, here depicted as Ba-122, are widely used [9]-[15]. These crystals have high quality monocrystals and are easily to obtain. Very important that for these crystals was easy to produce SC materials with a variety of chemical substitutions. The SC phase was first observed by Co substitution on the Fe site [9]. The parent compound is a paramagnetic semimetal, it turns into superconductor upon electron doping by d-electrons atoms (substitution of Fe atoms by Co, Ni, Rh or Pd) or upon hole doping in the plane of the Ba atoms (e.g., substitution of Ba atoms by K). Also, the isovalent doping (substitution of Fe atoms by Ru) gives rise to SC state. On the other hand, some d-electron atoms: Cr [10], Mo [11] Mn [12] and Cu [13] [14] suppress the magnetism without stabilizing the high-T_c superconducting phase. To the best of our knowledge the reason for this is still unknown. The general features of the phase diagram are presented in **Figure 1**. As follows from Ref [15], the formation of a superconducting dome-like phase is observed with Rh at $T_c = 23.2$ K and with Pd at $T_c = 19$ K.

IBSC materials were intensively studied by theorists. It was shown that the IBSC materials have a quite complicated band structure and several disconnected Fermi surfaces (FSs) [16] [17] [18]. According to these studies all five 3d orbitals of the Fe are involved in the formation of the FSs. IBSC belong to the broad category of strongly correlated superconductors such as heavy fermions and cuprates high-T_c SC, although the latter have rather different mechanism of SC. We recommend the readers the popular and comprehensive reviews by Norman [19] [20], Mazin [21], Wang and Lee [22], Chubukov [23], Kordyuk [24], Baquero [25] and Prosorov *et al.* [26].

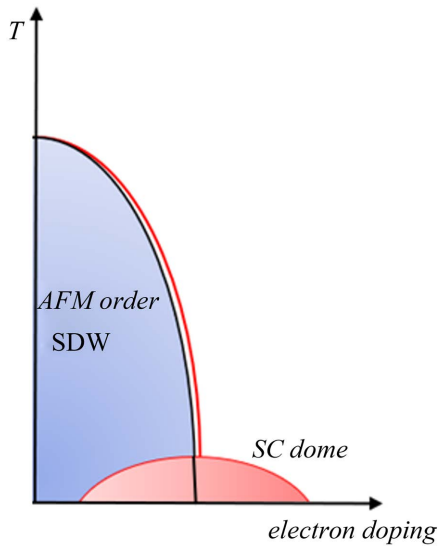

Figure 1. Phase diagram following from experiments [15] for $BaFe_2As_2$ doped by Rh and Pd.

From the first year of the discovery of the IBSC, it has been accepted that the superconductivity in these materials is non-conventional, presenting an antiferromagnetic (AFM) order, see also the article by Ouni *et al.* [27], where authors compared their DFT calculations with optical and vibrational properties. As was proposed by Mazin *et al.* [16] [17], the new superconducting materials tend to form AFM order, and the magnetism existing in the parent crystal at zero doping is suppressed by the AFM spin fluctuations, similar results were obtained also by Singh and Du [18]. The AFM spin fluctuations can induce s-wave pairing with sign change of the order parameter between the electron like FSs and hole like FSs, denoted as $s_{\pm}$. At the same time, Kuroki *at al.* [28] using random-phase approximation applied to the model of five d-orbitals obtained similar results as in Ref [16] [18], but they accepted the *d*-wave symmetry.

It is important to mention that basing on the five d-orbital model [28], Onari and Kontani [29], came to the conclusion that the interband impurity scattering is promoted by the d-orbital degree of freedom. Next year the authors [30] proposed a mechanism where an s_{++}-wave pairing was induced by orbital fluctuation they presenting arguments opposing to the $s_{\pm}$-wave pairing.

In another interesting approach, the IBSC materials were considered as some kind of Mott insulator [31] [32] [33]. The physics of the Mott insulators, which was elaborated before the discovery of the IBSC materials, may play an important role in the superconducting mechanism. If the IBSC materials are considered as doped Mott insulators, the anti-ferromagnetism and $s_{\pm}$-wave pairing will appear. As was discussed in the review by Lee *et al.* [34], the Anderson resonating valence bond theory that was first proposed for cuprates can be applied to the Mott insulating model.

The RVB theory [35] for high T_c superconductors was proposed by Anderson just after the discovery of the cuprates. In his theory, the antiferromagnetic lattice is melted into a spin-liquid phase composed by singlet pairs. When doping is applied, the singlets become charged giving rise to the superconducting state. His theory takes into account the separation between spin and charge, then the electronic excitation spectra can be presented as two different branches: charge spinless holons and chargeless spinons [36] [37].

In our previous publications [38] [39] [40] [41] we performed the comparative studies of the electronic structure of the pure $BaFe_2As_2$ and doped with substitutions of Fe atom by different d-electron atoms, using the Embedded Cluster Method at the restricted open shell Möller-Plesset second order (ECM-ROMP2) electron correlation level [42] [43] [44].

The charge and spin distributions we have obtained at the Natural Population Analysis level [45]. The found in our computer experiments peculiarities of the electronic structure of Fe-based superconductors, when we have used different dopants, for instance, the presence of spinless electron on the 3d orbitals, pointed out on the Anderson resonance valence bond (RVB) model as the possible mechanism for superconductivity for IBSC materials.

In the current article we present our results for the electronic structure of the

embedded $Ba_4Fe_5As_8$ cluster doped by Rh and Pd. The calculations were carried out at the electron correlation level using restricted open shell Möller-Plesset second order (RO-MP2) method. Calculations were performed by the MOLPRO 2021 [46] [47] suite of programs.

2. Methodology

In our calculations, the embedded cluster method ECM-ROMP2 at the electron correlation level [42] [43] [44] was used. In this approach, the influence of the spin contamination is avoided. The methodology ECM-ROMP2 consists by two stages. In the first part, the cluster representing the crystal is selected and quantum-mechanical calculations at the RO-MP2 electron correlation level are performed with the restricted open shell Hartree-Fock (RHF) method as the zero-order approximation. A detailed description of UMP2 and RO-MP2 is given in Appendix 3 of book [48]. The selected cluster preserved the symmetry of the crystal (D_2) and is presented in **Figure 2**.

At the second stage, the cluster is embedded in a background charges distribution that reproduces the Madelung potential for the infinite crystal on each cluster site. The symmetry of the crystal must be preserved and the cluster with the background charges must be neutral. The background charges are taken from our previous studies [38] [39] [40]. Then the cluster with the background charges is calculated at the RO-MP2 level. The charges are then modified and the whole system is recalculated, repeating this process until self-consistency is achieved, see Ref. [42]. The calculation scheme is presented on **Figure 3**.

The calculations are performed with the MOLPRO 2021 [46] [47] suite of programs. For Fe and As all electrons are taken into account. We use the triple split valence basis set with polarization and diffuse gaussian functions, 6-31G(d, p) [49] for Fe atoms and the 6-311G(d, p) [50] for As. These basis sets were provided by the Basis Set Exchange data base [51] [52] [53]. On the other hand, for Ba, Rh and Pd, the Wood-Boring pseudopotentials [54] [55] are employed and they are included in the MOLPRO 2020.1 suite of programs. For Ba we use ECP46MWB [56] and for Rh and Pd we use the ECP28MWB [57].

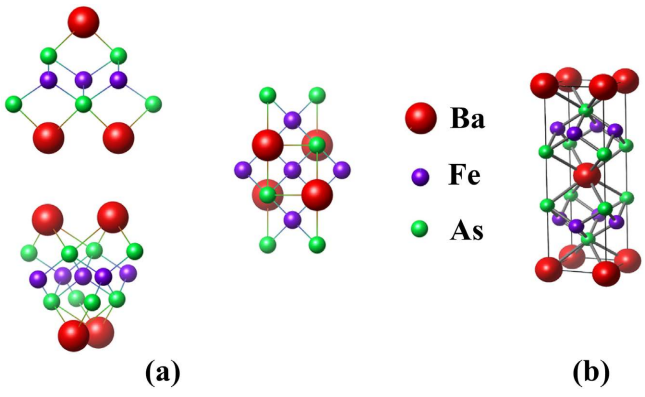

Figure 2. Structure of the cluster. (a) Different views of the cluster $Ba_4Fe_5As_8$. (b) The unit cell $Ba_2Fe_2As_2$.

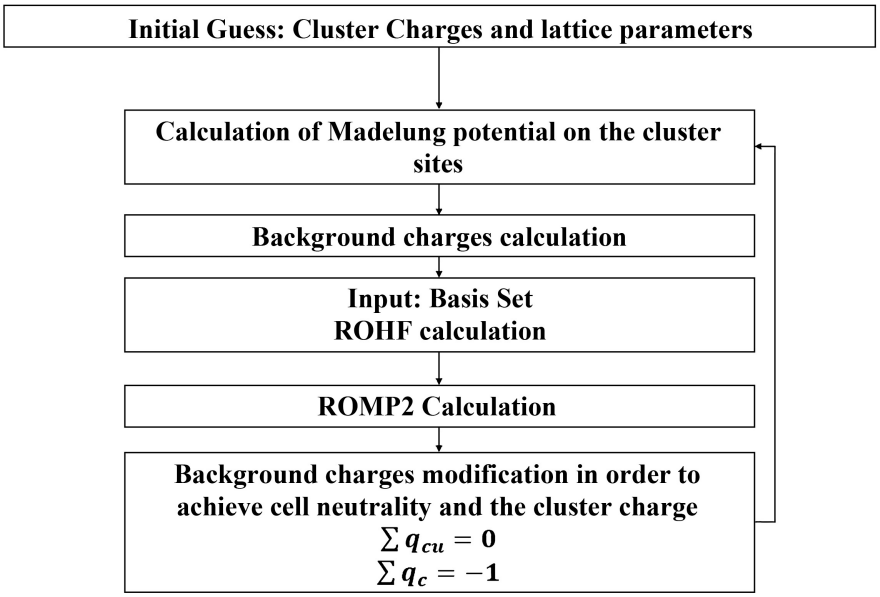

Figure 3. Iteration scheme used in our calculation.

After the calculations using the afore mentioned method are done, we analyze the orbital population using NPA by means of the Janpa software [58] [59].

3. Results and Discussions

In **Table 1** we present the pure and doped cluster energy calculated according to its multiplicity using MOLPRO 2020.1. For the pure cluster the ground state corresponds to multiplicity[1] $M = 2$ ($S = 1/2$). Since we are using restricted open shell method all the eigenvalues[2], of the $\widehat{S^2}$ operator, are exact. The ground state of the cluster doped by Rh is $M = 3$ ($S = 1$) and for Pd is $M = 2$ ($S = 1/2$).

According to **Table 1**, the ground state for the isolated pure cluster is $M = 6$ ($S = 5/2$). For Rh doping the ground state is $M = 5$ ($S = 2$) and for Pd doping the ground state is $M = 4$ ($S = 3/2$). Let us mention, that the change in the ground state for isolated and embedded cluster is associated with the inclusion of the background charge distribution. In the following subsection the Natural Population Analysis (NPA) to the calculated ground state embedded clusters will be presented.

Let us note that the energy of the cluster depends on the initial orbital population guess. According to MOLPRO manual [60], for high spin clusters the number of orbital population combinations that minimize the energy is greatly increased, and the software cannot perform this task automatically. Therefore, a manual search for minimal energy configuration was made and only the lower energy is reported here.

The atomic charge and the generalized valence orbital population obtained from the NPA analysis that is part of the NBO analysis are presented in **Table 2**, for RO-MP2 approach. In it only values for the atoms nearest neighbors (n.n.) to

[1]The multiplicity $M = 2S + 1$.

[2]The eigenvalue of the $\widehat{S^2}$ operator is equal to $S(S + 1)$.

Table 1. Energy of the states calculated at the RO-MP2 level using MOLPRO 2021.2 according to different multiplicities for the embedded and isolated cluster, pure and doped.

Multiplicity	Embedded Cluster (MOLPRO RO-MP2)		Isolated Cluster (MOLPRO RO-MP2)	
$Ba_4Fe_5As_8$	Energy (a.u.)	S^2 ($\hbar^2$)	Energy (a.u.)	S^2 ($\hbar^2$)
2	−24288.8038001	0.75 (0.75)	−24286.86140	0.75 (0.75)
4	−24288.1955127	3.75 (3.75)	−24287.14783	3.75 (3.75)
6	−24287.9551222	8.75 (8.75)	−24287.72156	8.75 (8.75)
8	−24288.0924433	15.75 (15.75)	−24286.57866	15.75 (15.75)
$Ba_4Fe_4RhAs_8$				
1	−23135.7686462	0 (0)	−23134.14784	0 (0)
3	−23137.1645838	2 (2)	−23133.63805	2 (2)
5	−23136.6737546	6 (6)	−23135.19875	6 (6)
7	−23136.4913259	12 (12)	−23134.03125	12 (12)
$Ba_4Fe_4PdAs_8$				
2	−23154.8427642	0.75 (0.75)	−23150.69902	0.75 (0.75)
4	−23153.1261771	3.75 (3.75)	−23152.54293	3.75 (3.75)
6	−23153.7146883	8.75 (8.75)	−23151.60083	8.75 (8.77)
8	−23153.2263467	15.75 (15.75)	−23151.78103	15.75 (15.87)

Table 2. Charge distribution at the ground state by the RO-MP2 method in pure and doped $Ba_4Fe_5As_8$ cluster, by NPA analysis using MOLPRO.

	Atomic Charge	Valence orbital population
$Ba_4Fe_5As_8$		$S = 1/2$
Fe	0.64	$4s^{0.46}3d^{6.57}$
Fe(n.n.)a	0.99	$4s^{0.49}3d^{6.42}$
Fe(n.n.)b	0.29	$4s^{0.61}3d^{7.77}$
As(n.n.)	−1.71	$4s^{1.54}4p^{4.92}$
$Ba_4Fe_4RhAs_8$		$S = 2$
Rh	−1.62	$5s^{0.29}4d^{7.42}5p^{1.92}$
Fe(n.n.)a	1.10	$4s^{0.52}3d^{6.08}$
Fe(n.n.)b	0.16	$4s^{1.12}3d^{4.9}$
As(n.n.)	−1.15	$4s^{1.7}4p^{4.69}$
$Ba_4Fe_4PdAs_8$		$S = 1/2$
Pd	−1.81	$5s^{0.25}4d^{8.8}5p^{1.98}$
Fe(n.n.)a	0.91	$4s^{0.45}3d^{6.59}$
Fe(n.n.)b	0.22	$4s^{0.68}3d^{5.9}$
As(n.n.)	−1.10	$4s^{1.67}4p^{4.58}$

the central atom are showed. The outer atoms of As and Ba are not presented since they are in the boundary of the cluster. We substitute the central atom of

the cluster by the dopant. The excited Rydberg orbitals are not presented, but they are taken into account for calculating the atomic charges.

According to Table 2 the charge in the central atom for the pure material is 0.64e. After doping a large negative charge appear on both dopant atoms. The negative charge for the As(n.n.) decreases upon doping and it is associated with the electron transfer from this atom to the dopant. In all Fe(n.n.) there is a small change in their charge. Thus, there is a charge transfer from As(n.n.) and Fe(n.n.)b atoms to dopants. This effect is related to the screening effect, since a large Z atom is being introduced into the cluster replacing the Fe atom.

We compare the valence orbital population of the atoms in the undoped cluster with the valence orbital population of free atoms: Fe: $[Ar]3d^6 4s^2$ and As: $[Ar]4s^2 4p^3$. According to Table 2, the Fe atoms in the pure cluster show a decrease on its 4s orbital population of 1.54e for the central atom, 1.51e for the Fe(n.n.)a and 1.39e for the Fe(n.n.)b. The population on the 3d orbitals is increased, 0.57e for the central atom, 0.42e for the Fe(n.n.)a, and 1.77e for the Fe(n.n.)b. At the As(n.n) atoms a decrease is observed in the 4s orbital population of 0.46e and an increase of 1.92e in the orbital 4p.

For comparing the valence orbital population of the isolated atom Rh: $[Kr]4d^8 5s^1$ with the Rh doped crystal, as follows from Table 2, a decrease on the 5s orbital population of 0.71e, of 0.58e in the 4d orbital and an increase of 1.92e for the 5p orbital population is observed. The population for the Fe(n.n.) in both directions decreases. For As(n.n.) a decrease of 0.3e and an increase of 1.69e in the 4s and 4p orbital population respectively is observed. The charge transfers from As(n.n.) atoms to the central atom Rh.

When doping with Pd, with electronic structure $[Kr]4d^{10}$, it is observed a decrease of 1.2e in the 4d orbital population, an increase in the 5s of 0.25e and also an increase of 1.98e for the 5p orbital population. For the nearest neighbor atoms, a decrease is observed in the population for the Fe(n.n.) in both directions. For As(n.n.) a decrease of 0.33e and an increase of 1.58e in the 4s and 4p orbital population respectively is observed. Just like in the Rh doping, it is observed a charge transfer from As(n.n.) atoms to the central Pd and a rearrangement of the orbital population in Pd, due to a significant population on Rydberg orbitals.

In Table 3, the data of the detailed valence orbital population RO-MP2 for the pure and doped cluster in its ground state is presented. When doping with Rh, the 5p orbital population is distributed uniformly in all directions. The 4d orbitals on the dopant are occupied by at least one electron. The Fe(n.n.)a exhibit a population decrease on d_{yz} and $d_{x^2-y^2}$, an increase on d_{xz}, whereas the others remain the same upon the Rh doping. In the Fe(n.n.)b atom it is observed an increase on the d_{xz} orbital population, a decrease on d_{xz}, d_{yz} and to the zero population on d_{z^2}, remaining the same for $d_{x^2-y^2}$. For the calculation by MOLPRO program and in the case of doping with Pd it is observed that the 5p orbital population of Pd is distributed homogeneously in all directions. The 4d

Table 3. Detailed charge orbital population for 3d(Fe), 4d(Rh, Pd), 5p(Rh, Pd) and 4p(As) at the ground state by the RO-MP2 method for pure and doped $Ba_4Fe_5As_8$ clusters by NPA analysis using MOLPRO.

$Ba_4Fe_5As_8$	$S = 1/2$
Fe	$d_{xy}^{1.37} + d_{xz}^{0.06} + d_{yz}^{1.93} + d_{x^2-y^2}^{1.58} + d_{z^2}^{1.63}$
Fe(n.n.)a	$d_{xy}^{1.03} + d_{xz}^{0.5} + d_{yz}^{1.38} + d_{x^2-y^2}^{1.76} + d_{z^2}^{1.75}$
Fe(n.n.)b	$d_{xy}^{1.56} + d_{xz}^{0.72} + d_{yz}^{1.81} + d_{x^2-y^2}^{1.84} + d_{z^2}^{1.84}$
As(n.n.)	$p_x^{1.6} + p_y^{1.66} + p_z^{1.66}$
$Ba_4Fe_4RhAs_8$	$S = 2$
Rh	$d_{xy}^{1.72} + d_{xz}^{1.16} + d_{yz}^{1.45} + d_{x^2-y^2}^{1.29} + d_{z^2}^{1.8}$ $p_x^{0.52} + p_y^{0.63} + p_z^{0.77}$
Fe(n.n.)a	$d_{xy}^{1.11} + d_{xz}^{1.1} + d_{yz}^{1.03} + d_{x^2-y^2}^{1.04} + d_{z^2}^{1.8}$
Fe(n.n.)b	$d_{xy}^{1.01} + d_{xz}^{1.03} + d_{yz}^{1.01} + d_{x^2-y^2}^{1.85} + d_{z^2}^{0}$
As(n.n.)	$p_x^{1.69} + p_y^{1.5} + p_z^{1.5}$
$Ba_4Fe_4PdAs_8$	$S = 1/2$
Pd	$d_{xy}^{1.74} + d_{xz}^{1.71} + d_{yz}^{1.74} + d_{x^2-y^2}^{1.68} + d_{z^2}^{1.93}$ $p_x^{0.66} + p_y^{0.55} + p_z^{0.77}$
Fe(n.n.)a	$d_{xy}^{1.53} + d_{xz}^{1.44} + d_{yz}^{0.98} + d_{x^2-y^2}^{1.15} + d_{z^2}^{1.49}$
Fe(n.n.)b	$d_{xy}^{1.59} + d_{xz}^{0.71} + d_{yz}^{1.78} + d_{x^2-y^2}^{1.82} + d_{z^2}^{0}$
As(n.n.)	$p_x^{1.5} + p_y^{1.54} + p_z^{1.54}$

orbitals are almost fully occupied in all directions. In Fe(n.n.)a, the orbital population on d_{yz}, $d_{x^2-y^2}$ and d_{z^2} orbitals, is increased, and on d_{xz} and d_{xy} orbitals its population is decreased upon doping. In the Fe(n.n.)b atom it is observed a decrease to zero on the d_{z^2} orbital population whereas all other directions remain the same when doping.

In Table 4 and Table 5 we present the spin distribution calculated at RO-MP2 electron correlation level. It is observed that the spin on central Fe is $0.72\hbar$. The spin practically disappears on all atoms when doping with Pd. According to the results obtained, there is no apparent spin transfer direction when doping. Let us note that the zero-spin density on all orbitals of the dopant is in agreement with the charge populations in both dopants.

As follows from Table 3 and Table 5, the orbitals d_{yz} and $d_{x^2-y^2}$ of Fe(n.n.)a, and d_{xz} of Fe(n.n.)b for Pd doping are practically occupied by one electron with zero spin population. Whereas, for the orbitals $d_{x^2-y^2}$ of Fe(n.n.)b for Rh doping a charge population of 2e is observed with spin $S = 1/2$. The presence of one electron charge on the orbital population with no component of spin is observed. This is in agreement with the spinless holons proposed by Anderson in his RVB model of high T_c-SC [35] [36] [37].

Table 4. NPA spin distribution at the ground state of the embedded cluster, pure and doped, at the RO-MP2 level.

	Spin ($\hbar$)	Valence orbital spin population
$Ba_4Fe_5As_8$		$S = 1/2$
Fe	0.72	$4s^{0}3d^{0.71}$
Fe(n.n.)a	0.03	$4s^{0.01}3d^{0.04}$
Fe(n.n.)b	−0.05	$4s^{0.03}3d^{-0.05}$
As(n.n.)	0.04	$4s^{0}4p^{0.08}$
$Ba_4Fe_4RhAs_8$		$S = 2$
Rh	1.61	$5s^{0.01}4d^{1.46}5p^{0.24}$
Fe(n.n.)a	3.86	$4s^{0.04}3d^{3.84}$
Fe(n.n.)b	−4.62	$4s^{0.14}3d^{-3.88}$
As(n.n.)	0.18	$4s^{0}4p^{0.37}$
$Ba_4Fe_4PdAs_8$		$S = 1/2$
Pd	0.08	$5s^{0.01}4d^{-0.08}5p^{0.16}$
Fe(n.n.)a	−0.03	$4s^{-0.01}3d^{-0.01}$
Fe(n.n.)b	0.01	$4s^{0.02}3d^{0.02}$
As(n.n.)	0.07	$4s^{-0.01}4p^{0.06}$

Table 5. Detailed spin orbital population for 3d(Fe), 4d(Rh, Pd), 5p(Rh, Pd) and 4p(As)at the ground state of the embedded cluster, pure and doped, at the RO-MP2 level.

$Ba_4Fe_5As_8$	$S = 1/2$
Fe	$d_{xy}^{0.59} + d_{xz}^{0} + d_{yz}^{0.01} + d_{x^2-y^2}^{-0.24} + d_{z^2}^{0.35}$
Fe(n.n.)a	$d_{xy}^{0.09} + d_{xz}^{-0.04} + d_{yz}^{0} + d_{x^2-y^2}^{0} + d_{z^2}^{-0.01}$
Fe(n.n.)b	$d_{xy}^{-0.04} + d_{xz}^{-0.02} + d_{yz}^{0.01} + d_{x^2-y^2}^{0} + d_{z^2}^{0}$
As(n.n.)	$p_x^{0.04} + p_y^{0.04} + p_z^{0}$
$Ba_4Fe_4RhAs_8$	$S = 2$
Rh	$d_{xy}^{0.22} + d_{xz}^{0.24} + d_{yz}^{0.31} + d_{x^2-y^2}^{0.53} + d_{z^2}^{0.16}$ $p_x^{0.08} + p_y^{0.11} + p_z^{0.05}$
Fe(n.n.)a	$d_{xy}^{0.87} + d_{xz}^{0.88} + d_{yz}^{0.95} + d_{x^2-y^2}^{0.94} + d_{z^2}^{0.2}$
Fe(n.n.)b	$d_{xy}^{-0.86} + d_{xz}^{-0.97} + d_{yz}^{-0.95} + d_{x^2-y^2}^{-0.97} + d_{z^2}^{-0.13}$
As(n.n.)	$p_x^{0.09} + p_y^{0.14} + p_z^{0.14}$
$Ba_4Fe_4PdAs_8$	$S = 1/2$
Pd	$d_{xy}^{0.12} + d_{xz}^{0.01} + d_{yz}^{0.02} + d_{x^2-y^2}^{0} + d_{z^2}^{0.01}$ $p_x^{-0.02} + p_y^{-0.03} + p_z^{-0.03}$
Fe(n.n.)a	$d_{xy}^{-0.09} + d_{xz}^{0.02} + d_{yz}^{0.02} + d_{x^2-y^2}^{-0.01} + d_{z^2}^{0.05}$
Fe(n.n.)b	$d_{xy}^{0} + d_{xz}^{-0.03} + d_{yz}^{0.01} + d_{x^2-y^2}^{0.02} + d_{z^2}^{-0.02}$
As(n.n.)	$p_x^{0.02} + p_y^{0} + p_z^{0.04}$

4. Concluding Remarks

A charge transfer from the As and Fe(n.n.)b atoms to the central atoms was observed for both dopants. From our tables follows asymmetries in the occupancy of the Fe(n.n.) 3d orbitals in a and b directions. Also follows from our tables that the charge transfers from nearest neighbor atoms to the central dopants, while there was no evident direction of spin transfer.

It is important to mention that for Pd dopant, the spin disappears on the dopant whereas for Rh dopant there is a spin population different from cero. From this follows that charge and spin transfer are completely independent. According to the calculated charge and spin orbital distributions, it follows the existence of spinless electrons (Anderson's holon). This indicates the possibility of the superconductivity mechanism in this material proposed by Anderson in his RVB theory.

The IBSC material studied in our paper is consisting of planes of $(FeAS)_2$. Upon doping on the planes appears charge transfer from Fe(n.n.)_b to the central atom in the selected cluster. The modified orbitals are projected perpendicular to the plane. It would be interesting to study, using a five-band orbital Hubbard model, the behavior of these atoms in the proposed configuration of our cluster.

Acknowledgements

The authors thank to the DGTIC computer staff for providing access to the MITZLI cluster Universidad Nacional Autónoma de México. This work was partly supported by grant from DGAPA PAPIT IN111519. We also thank to Lic. Inf. Alejandro Pompa-García and Tec. Cain González for technical support.

Data Availability

The data that support the findings of this study are available from the corresponding author upon reasonable request.

Conflicts of Interest

The authors have no conflicts to disclose.

References

[1] Kamerling Onnes, H. (1911) On the Change in the Resistance of Pure Metals at Very Low Temperatures. III. The Resistance of Platinum at Helium Temperatures. *Communications*, **124**, 799-802.

[2] Heisenberg, W. (1925) Quantum-Theoretical Re-Interpretation of Kinematic and Mechanical Relations. *Zeitschrift für Physik*, **33**, 879-893. https://doi.org/10.1007/BF01328377

[3] Born, M. and Jordan, P. (1925) Zur Quantenmechanik. *Zeitschrift für Physik*, **34**, 858-888. https://doi.org/10.1007/BF01328531

[4] Schrödinger, E. (1926) On the Relation between the Quantum Mechanics of Heisenberg, Born, and Jordan, and that of Schrödinger. *Annalen der Physik*, **79**,

361-376, 489-527, 734-756. https://doi.org/10.1002/andp.19263840804

[5] Schrödinger, E. (1926) An Undulatory Theory of the Mechanics of Atoms and Molecules. *Physical Review*, **28**, 1049-1070. https://doi.org/10.1103/PhysRev.28.1049

[6] Kamihara, Y., Watanabe, M. and Hosono, H. (2008) Iron-Based Layered Superconductor La[$O_{1-x}F_x$]FeAs (x = 0.05-0.12) with T_c = 26 K. *Journal of the American Chemical Society*, **130**, 3296-3297. https://doi.org/10.1021/ja800073m

[7] Takahashi, H., Igawa, K., Arii, K., Kamihara, Y., Hirano, M. and Hosono, H. (2008) Superconductivity at 43 K in an Iron-Based Layered Compound $LaO_{1-x}F_xFeAs$. *Nature* (*London*), **453**, 376-378. https://doi.org/10.1038/nature06972

[8] Stewart, R.G. (2011). Superconductivity in Iron Compounds. *Reviews of Modern Physics*, **83**, 1589-1652. https://doi.org/10.1103/RevModPhys.83.1589

[9] Sefat, A.S., Jin, R., McGuire, M.A., Sales, B.C., Singh, D.J. and Mandrus, D. (2008) Superconductivity at 22 K in Co-Doped $BaFe_2As_2$ Crystals. *Physical Review Letters*, **101**, Article ID: 117004. https://doi.org/10.1103/PhysRevLett.101.117004

[10] Sefat, A.S., Singh, D.J., Van Bebber, L.H., *et al.* (2009) Absence of Superconductivity in Hole-Doped $BaFe_{2-x}CrxAs_2$ Single Crystals. *Physical Review B*, **79**, Article ID: 224524. https://doi.org/10.1103/PhysRevB.79.224524

[11] Sefat, A.S., Marty, K., Christianson, A.D., *et al.* (2012) Effect of Molybdenum 4d Hole Substitution in $BaFe_2As_2$. *Physical Review B*, **85**, Article ID: 024503. https://doi.org/10.1103/PhysRevB.85.024503

[12] Texier, Y., Laplace, Y., Mendels, P., *et al.* (2012) Mn Local Moments Prevent Superconductivity in Iron Pnictides $Ba(Fe_{1-x}Mn_x)_2As_2$. *Europhysics Letters,* **99**, 17002. https://doi.org/10.1209/0295-5075/99/17002

[13] Canfield, P.C., Bud'ko, S.L., Ni, N., Yan, J.Q. and Kracher, A. (2009) Decoupling of the Superconducting and Magnetic/Structural Phase Transitions in Electron-Doped $BaFe_2As_2$. *Physical Review B*, **80**, Article ID: 060501. https://doi.org/10.1103/PhysRevB.80.060501

[14] Mun, E.D., Bud'ko, S.L., Ni, N., Thaler, A.N. and Canfield, P.C. (2009) Thermoelectric Power and Hall Coefficient Measurements on $Ba(Fe_{1-x}T_x)_2As_2$ (T=Co and Cu). *Physical Review B*, **80**, Article ID: 054517.

[15] Ni, N., Thaler, A., Kracher, A., Yan, J.Q., Bud'ko, S.L. and Canfield, P.C. (2009) Phase Diagrams of $Ba(Fe_{1-x}M_x)_2As_2$ Single Crystals (M=Rh and Pd). *Physical Review B*, **80**, Article ID: 024511.

[16] Mazin, I.I., Singh, D.J., Johannes, M.D. and Du, M.H. (2008) Comment on "Low-Lying States and Hidden Kinematic Collective Charge Instabilities in Parent Cobaltate Superconductors. *Physical Review Letters*, **101**, Article ID: 057003. https://doi.org/10.1103/PhysRevLett.101.089703

[17] Mazin, I.I. and Schmalian, J. (2009) Pairing Symmetry and Pairing State in Ferropnictides: Theoretical Overview. *Physica C*, **469**, 614-627. https://doi.org/10.1016/j.physc.2009.03.019

[18] Singh, D.J. and Du, M.H. (2008) Density Functional Study of $LaFeAsO_{1-x}F_x$: A Low Carrier Density Superconductor near Itinerant Magnetism. *Physical Review Letters*, **100**, Article ID: 237003. https://doi.org/10.1103/PhysRevLett.100.237003

[19] Norman, M.R. (2008) High-Temperature Superconductivity in the Iron Pnictides. *Physics*, **1**, Article No. 21. https://doi.org/10.1103/Physics.1.21

[20] Mazin, I.I. (2010) Superconductivity Gets an Iron Boost. *Nature*, **464**, 183-186. https://doi.org/10.1038/nature08914

[21] Norman, M.R. (2011) The Challenge of Unconventional Superconductivity. *Science*,

332, 196-200. https://doi.org/10.1126/science.1200181

[22] Wang, F. and Lee, D.H. (2011) The Electron-Pairing Mechanism of Iron-Based Superconductors. *Science*, **332**, 200-204. https://doi.org/10.1126/science.1200182

[23] Chubukov, A. (2012) Pairing Mechanism in Fe-Based Superconductors. *Annual Review of Condensed Matter Physics*, **3**, 57-92. https://doi.org/10.1146/annurev-conmatphys-020911-125055

[24] Kordyuk, A.A. (2012) Iron-Based Superconductors: Magnetism, Superconductivity, and Electronic Structure (Review Article). *Low Temperature Physics*, **38**, 888. https://doi.org/10.1063/1.4752092

[25] Baquero, R. (2014) La Superconductividad: sus orígenes, sus teorías, sus problemas candentes hoy. *Revista de la Academia Colombiana de Ciencias Exactas*, **38**, 18-33. https://doi.org/10.18257/raccefyn.152

[26] Prozorov, R., Kończykowski, M., Tanatar, M.A., Wen, H.H., Fernandes, R.M. and Canfield, P.C. (2019) Interplay between Superconductivity and Itinerant Magnetism in Underdoped $Ba_{1-x}K_xFe_2As_2$ ($x = 0.2$) Probed by the Response to Controlled Point-Like Disorder. *NPJ Quantum Materials*, **4**, Article No. 34. https://doi.org/10.1038/s41535-019-0171-2

[27] Ouni, B., Larbi, T. and Amlouk, M. (2022) Vibrational, Electronic and Structural Study of Sprayed ZnO Thin Film Based on the IR-Raman Spectra and DFT Calculations. *Crystal Structure Theory and Applications* **11**, 23-38. https://doi.org/10.4236/csta.2022.112002

[28] Kuroki, K., Onari, S., Arita, R., Usui, H., *et al.* (2008) Unconventional Pairing Originating from the Disconnected Fermi Surfaces of Super-conducting $LaFeAsO_{1-x}F_x$. *Physical Review Letters*, **101**, Article ID: 087004. https://doi.org/10.1103/PhysRevLett.101.087004

[29] Onari, S. and Kontani, H. (2009) Violation of Anderson's Theorem for the Sign-Reversing S-Wave State of Iron-Pnictide Superconductors. *Physical Review Letters*, **103**, Article ID: 177001. https://doi.org/10.1103/PhysRevLett.103.177001

[30] Kontani, H. and Onari, S. (2010) Orbital-Fluctuation-Mediated Superconductivity in Iron Pnictides: Analysis of the Five-Orbital Hubbard-Holstein Model. *Physical Review Letters*, **104**, Article ID: 157001. https://doi.org/10.1103/PhysRevLett.104.157001

[31] Chen, W.Q., Yang, K.Y., Zhou, Y. and Hang, F.C. (2009) Strong Coupling Theory for Superconducting Iron Pnictides. *Physical Review Letters*, **102**, Article ID: 047006. https://doi.org/10.1103/PhysRevLett.102.047006

[32] Qazilbash, M.M., Hamlin, J.J., Baumbach, R.E., Zhang, L., Singh, D.J., Maple, M.B. and Basov, D.N. (2009) Electronic Correlations in the Iron Pnictides. *Nature Physics*, **5**, 647-650. https://doi.org/10.1038/nphys1343

[33] Laad, M.S., Craco, L., Leoni, S. and Rosner, H. (2009) Electrodynamic Response of Incoherent Metals: Normal Phase of Iron Pnictides. *Physical Review B*, **79**, Article ID: 024515. https://doi.org/10.1103/PhysRevB.79.024515

[34] Lee, P.A., Nagaosa, N. and Wen, X.G. (2006) Doping a Mott Insulator: Physics of High-Temperature Superconductivity. *Reviews of Modern Physics*, **78**, 17-85. https://doi.org/10.1103/RevModPhys.78.17

[35] Anderson, P.W. (1987) The Resonating Valence Bond State in La_2CuO_4 and Superconductivity. *Science*, **235**, 1196-1198. https://doi.org/10.1126/science.235.4793.1196

[36] Kivelson, S.A., Rokhsar, D.S. and Sethna, J.P. (1987) Topology of the Resonating

Valence-Bond State: Solitons and High-Tc Superconductivity. *Physical Review B*, **35**, 8865-8868. https://doi.org/10.1103/PhysRevB.35.8865

[37] Anderson, P.W., Baskaran, G., Zou, Z. and Hsu, T. (1987) Resonating-Valence-Bond Theory of Phase Transitions and Superconductivity in La_2CuO_4-Based Compounds. *Physical Review Letters*, **58**, 2790-2793. https://doi.org/10.1103/PhysRevLett.58.2790

[38] Soullard, J., Pérez-Enriquez, R. and Kaplan, I. (2015) Comparative Study of Pure and Co-Doped $BaFe_2As_2$. *Physical Review B*, **91**, Article ID: 184517. https://doi.org/10.1103/PhysRevB.91.184517

[39] Soullard, J. and Kaplan, I. (2016) Comparative Study of the Magnetic Structure of $BaFe_2As_2$ Doped with Co or Ni. *Journal of Superconductivity and Novel Magnetism*, **29**, 3147-3154. https://doi.org/10.1007/s10948-016-3626-8

[40] Columbié-Leyva, R., Soullard, J. and Kaplan, I. (2019) Electronic Structure Study of New Family of High-T_c Fe-Superconductors Based on $BaFe_2As_2$ in Presence of Dopants Rh and Pd. *MRS Advances*, **4**, 3365-3372. https://doi.org/10.1557/adv.2019.409

[41] Columbié-Leyva, R., Miranda, U., López-Vivas, A., Soullard, J. and Kaplan, I.G. (2021) Quantum Mechanical Calculations of High-T_c Fe-Superconductors. *Journal of Quantum Information Science*, **11**, 84-98. https://doi.org/10.4236/jqis.2021.112007

[42] Kaplan, I.G., Soullard, J., Hernández-Cobos, J. and Pandey, R. (1999) Electronic Structure of $YBa_2Cu_3O_7$ Ceramics at the MP2 Electron Correlation Level. *Journal of Physics*: *Condensed Matter*, **11**, 1049-1058. https://doi.org/10.1088/0953-8984/11/4/012

[43] Kaplan, I.G., Hernández-Cobos, J. and Soullard, J. (1998) Quantum Systems in Chemistry and Physics, Kluwer Academic, Dordrecht, 143-158.

[44] Kaplan, I.G., Soullard, J. and Hernández-Cobos, J. (2002) Effect of Zn and Ni Substitution on the Local Electronic Structure of the $YBa_2Cu_3O_7$ Superconductor. *Physical Review B*, **65**, Article ID: 214509. https://doi.org/10.1103/PhysRevB.65.214509

[45] Foster, J.P. and Weinhold, F. (1980) Natural Hybrid Orbitals. *Journal of the American Chemical Society*, **102**, 7211-7218. https://doi.org/10.1021/ja00544a007

[46] Werner, H.-J., Knowles, P.J., Knizia, G., Manby, F.R. and Schütz, M. (2012) Molpro: a General-Purpose Quantum Chemistry Program Package. *WIREs Computational Molecular Science*, **2**, 242-253. https://doi.org/10.1002/wcms.82

[47] Werner, H.-J., Knowles, P.J., *et al.* (2020) The Molpro Quantum Chemistry Package. *The Journal of Chemical Physics*, **152**, Article ID: 144107. https://doi.org/10.1063/5.0005081

[48] Kaplan, I.G. (2006) Intermolecular Interaction: Physical Picture, Computational Methods and Model Potentials. John Wiley & Sons, Chichester, 367. https://doi.org/10.1002/047086334X

[49] Rassolov, V.A., Pople, J.A., Ratner, M.A. and Windus, T.L. (1998) 6-31G* Basis Set for Atoms K through Zn. *The Journal of Chemical Physics*, **109**, 1223-1229. https://doi.org/10.1063/1.476673

[50] Curtiss, L.A., McGrath, M.P., Blaudeau, J.-P., Davis, N.E., Binning, R.C. and Radom, L. (1995) Extension of Gaussian-2 Theory to Molecules Containing Third-Row Atoms Ga-Kr. *The Journal of Chemical Physics*, **103**, 6104-6113. https://doi.org/10.1063/1.470438

[51] Pritchard, B.P., Altarawy, D., Didier, B., Gibsom, T.D. and Windus, T.L. (2019)

New Basis Set Exchange: An Open, Up-to-Date Resource for the Molecular Sciences Community. *Journal of Chemical Information and Modeling*, **59**, 4814-4820. https://doi.org/10.1021/acs.jcim.9b00725

[52] Feller, D. (1996) The Role of Databases in Support of Computational Chemistry Calculations. *Journal of Computational Chemistry*, **17**, 1571-1586. https://doi.org/10.1002/(SICI)1096-987X(199610)17:13<1571::AID-JCC9>3.0.CO;2-P

[53] Schuchardt, K.L., Didier, B.T., Elsethagen, T., *et al.* (2007) Basis Set Exchange: A Community Database for Computational Sciences. *Journal of Chemical Information and Modeling*, **47**, 1045-1052. https://doi.org/10.1021/ci600510j

[54] Dolg, M., Stoll, H., Savin, A. and Preuss, H. (1989) Energy-Adjusted Pseudopotentials for the Rare Earth Elements. *Theoretical Chemistry Accounts*, **75**, 173-194. https://doi.org/10.1007/BF00528565

[55] Küchle, W., Dolg, M., Stoll, H. and Preuss, H. (1994) Energy-Adjusted Pseudopotentials for the Actinides. Parameter Sets and Test Calculations for Thorium and Thorium Monoxide. *The Journal of Chemical Physics*, **100**, 7535-7542. https://doi.org/10.1063/1.466847

[56] Kaupp, M., Schleyer, P.V.R., Stoll, H. and Preuss, H. (1991) Pseudopotential Approaches to Ca, Sr, and Ba Hydrides. Why Are Some Alkaline Earth MX_2 Compounds Bent? *The Journal of Chemical Physics*, **94**, 1360-1366. https://doi.org/10.1063/1.459993

[57] Andrae, D., Haeussermann, U., Dolg, M., Stoll, H. and Preuss, H. (1990) Energy-Adjusted *ab initio* Pseudopotentials for the Second and Third Row Transition Elements. *Theoretical Chemistry Accounts*, **77**, 123-141. https://doi.org/10.1007/BF01114537

[58] Nikolaienko, T.Y. and Bulavin, L.A. (2019) Localized Orbitals for Optimal Decomposition of Molecular Properties. *International Journal of Quantum Chemistry*, **119**, e25798. https://doi.org/10.1002/qua.25798

[59] Nikolaienko, T.Y., Bulavin, L.A. and Hovorun, D.M. (2014) JANPA: An Open Source Cross-Platform Implementation of the Natural Population Analysis on the Java Platform. *Computational and Theoretical Chemistry*, **1050**, 15-22. https://doi.org/10.1016/j.comptc.2014.10.002

[60] Werner, H.J. and Knowles, P.J. (2015) MOLPRO Users Manual, Version 2015.1. https://www.theochem.ru.nl/files/local/molpro2015.1.pdf